Eur. Phys. J. C (2022) 82:298
https://doi.org/10.1140/epjc/s10052-022-10274-4

THE EUROPEAN PHYSICAL JOURNAL C

Regular Article - Theoretical Physics

Stability analysis of circular orbits around a traversable wormhole with massless conformally coupled scalar field

Shobhit Giri[1,a], **Hemwati Nandan**[2,1,b], **Lokesh Kumar Joshi**[3,c], **Sunil D. Maharaj**[4,d]

[1] Department of Physics, Gurukula Kangri (Deemed to be University), Haridwar, Uttarakhand 249 404, India
[2] Center for Space Research, North-West University, Mahikeng 2745, South Africa
[3] Department of Applied Science, Faculty of Engineering and Technology, Gurukula Kangri (Deemed to be University), Haridwar, Uttarakhand 249 404, India
[4] Astrophysics Research Centre, School of Mathematics, Statastics and Computer Science, University of KwaZulu-Natal, Private Bag X54001, Durban 4000, South Africa

Received: 24 January 2022 / Accepted: 27 March 2022 / Published online: 5 April 2022
© The Author(s) 2022

Abstract We study the stability of circular orbits in the background of a traversable wormhole (TWH) spacetime obtained as a solution of Einstein's field equations coupled conformally to a massless scalar field. The Lyapunov stability approach is employed to determine the stability of circular orbits (timelike and null) of non-spinning test particles around a TWH spacetime. In the case of timelike geodesics, the particle is confined to move in four different types of effective potentials depending on various values of the angular momentum $\tilde{L}$ with both centrifugal and gravitational part. The effective potential for null geodesics consists of only a centrifugal part. Further, we characterize each fixed point according to its Lyapunov stability, and thus classify the circular orbits at the fixed point into stable center and unstable saddle points by depicting the corresponding phase-portraits.

1 Introduction

In view of general theory relativity (GR), Einstein and Rosen predicted the existence of bridges connecting two distant regions in spacetime named as Einstein–Rosen bridges or wormholes (WHs) [1,2]. Thereafter, the pioneering work of Morris and Thorne [3] developed the topological connections between separated regions of spacetime, as solutions of Einstein's field equations in GR, leading to the formation of three-dimensional TWH geometries. Such WHs are considered as static and spherically symmetric spacetimes connecting two asymptotically flat regions with different physical properties. In the last few decades, a variety of studies in various aspects including gravitational lensing by wormholes [4–7], shadows cast by WHs [8–10], accretion disks surrounding them [11–13], and their viability as black hole alternatives [14–16] have been widely investigated in detail. The violation of the null energy condition (NEC) [17,18] in the stress-energy tensor is required for construction of TWH which can be achieved by an exotic matter source responsible for the respective geometry [19–25]. In fact, there is no need of any exotic matter in order to obtain TWH spacetimes in many modified theories of gravity [26–29]. In order to avoid the presence of an exotic matter in such geometries, Barcelo and Visser [19] examined the conformal coupling of massless scalar field with gravity providing a large class of TWHs which also violate the NEC. They obtained a three-parameter class of exact solutions including the Schwarzschild geometry, certain naked singularities, and a collection of TWHs as analytical solutions of Einstein's field equations. In view of such a conformal coupling, Callan et al. [30] introduced a "new improved stress-energy tensor" to obtain an interesting set of TWHs. The new form of energy-momentum tensor which is also capable of violating the NEC for a massless conformal scalar field ϕ_c, is defined as

$$T_{\alpha\beta} = \nabla_\alpha\phi_c\nabla_\beta\phi_c - \frac{1}{2}g_{\alpha\beta}\left(\nabla\phi_c\right)^2 + \frac{1}{6}\Big[G_{\alpha\beta}\phi_c^2 - 2\nabla_\alpha\left(\phi_c\nabla_\beta\phi_c\right) + 2g_{\alpha\beta}\nabla^\mu\left(\phi_c\nabla_\mu\phi_c\right)\Big], \tag{1}$$

where, $G_{\alpha\beta}$ and $g_{\alpha\beta}$ represents Einstein's tensor and metric tensor of spacetime respectively.

In this article, we wish to focus attention on static and spherically symmetric TWH geometries which were obtained by Barcelo and Visser [19] by relating them conformally to the Janis–Newman–Winicour–Wyman (JNWW)

[a] e-mail: shobhit6794@gmail.com
[b] e-mail: hnandan@associates.iucaa.in (corresponding author)
[c] e-mail: lokesh.joshe@gmail.com
[d] e-mail: maharaj@ukzn.ac.za

solution [31–33]. The scalar field corresponding to JNWW solutions is represented by

$$\phi_m = \sqrt{\frac{(8\pi G_N)^{-1}}{2}} \sin\chi \, \ln\left(1-\frac{2\eta}{r}\right), \tag{2}$$

where G_N is Newton's constant. In spherical polar coordinates (t, r, θ, ϕ), Agnese et al. [34] obtained the JNWW metric as solutions of the Einstein field equations, minimally coupled to a massless scalar field ϕ_m, as given below

$$ds_m^2 = -\left(1-\frac{2\eta}{r}\right)^{\cos\chi} dt^2 + \left(1-\frac{2\eta}{r}\right)^{-\cos\chi} dr^2 + \left(1-\frac{2\eta}{r}\right)^{1-\cos\chi} r^2\left(d\theta^2+\sin^2\theta d\phi^2\right), \tag{3}$$

where parameters $\chi \in [0, \pi]$ and $\eta \geq 0$.

Considering the new improved energy-momentum tensor $T_{\alpha\beta}$, Barcelo and Visser [19] solved the Einstein's field equations

$$G_{\alpha\beta} = (8\pi G_N)\, T_{\alpha\beta}, \tag{4}$$

with $G_{\alpha\beta} = R_{\alpha\beta} - \frac{1}{2} g_{\alpha\beta} R$. Since $T_{\alpha\beta}$ is traceless for a conformal field i.e. $T_{\alpha\beta}\, g^{\alpha\beta} = 0$, then the scalar curvature $R = 0$. Thus the Einstein field equations coupled to conformal scalar field ϕ_c can be written as [19]

$$R_{\alpha\beta} = \left(\kappa - \frac{1}{6}\phi_c^2\right)^{-1}\left(\frac{2}{3}\nabla_\alpha\phi_c\nabla_\beta\phi_c - \frac{1}{6}g_{\alpha\beta}(\nabla\phi_c)^2 - \frac{1}{3}\phi_c\nabla_\alpha\nabla_\beta\phi_c\right), \tag{5}$$

$$\nabla^2\phi_c = 0. \tag{6}$$

Any metric ds conformal to the JNWW metric ds_m with conformal factor $\Omega(r)$ requires [20]

$$ds = \Omega(r) ds_m. \tag{7}$$

The conformal factor $\Omega(r)$ with two real constants γ_+ and γ_- can be expressed as [19]

$$\Omega(r) = \gamma_+\left(1-\frac{2\eta}{r}\right)^{\frac{\sin\chi}{2\sqrt{3}}} + \gamma_-\left(1-\frac{2\eta}{r}\right)^{-\frac{\sin\chi}{2\sqrt{3}}}. \tag{8}$$

We have a three-parameter set (χ, η, Δ), by defining an angle Δ, such that

$$\tan\frac{\Delta}{2} = \frac{\gamma_+ - \gamma_-}{\gamma_+ + \gamma_-} = \frac{\bar{\gamma_+} - 1}{\bar{\gamma_+} + 1}, \tag{9}$$

having range $\Delta \in (-\pi, \pi]$ and $\bar{\gamma_+} = \frac{\gamma_+}{\gamma_-}$.

One obtains various spacetime metrics depending on the choice of these parameters (i.e χ, η, Δ). The Schwarzschild black hole (SBH) metric can be recovered from ds^2 in the prescribed limit $\chi = 0$ and for arbitrary values of η and Δ.

We intend to investigate the stability of circular orbits of test particles in the vicinity of TWH spacetime conformally coupled to a massless scalar field by using Lyapunov (in)stability criteria (as discussed in [35] and references therein). Further, by analysing the phase-portrait in both cases of circular geodesics, we characterize each circular orbit at the fixed point as a stable center or an unstable saddle point. Boehmer et al. [36] extensively described two methods namely Lyapunov stability analysis [37] and Jacobi stability analysis [38], or the Kosambi–Cartan–Chern (KCC) theory [39–41] for analysing stability of a dynamical system which plays crucial role in gravitation and cosmology. The behavior of steady states of any dynamical system is analyzed to investigate the stability of the system. Lyapunov linear stability analysis requires the linearization of the dynamical system using the Jacobian matrix of a nonlinear system. However, both the linear and nonlinear stability analysis can be performed via Lyapunov stability approach [35,37]. Besides, the Jacobi stability or the KCC theory is formulated in terms of a deviation equation of a second-order differential equation defining the whole trajectory subject to small perturbations. The trajectories of the structure equations those bunch together are Jacobi stable while trajectories are Jacobi unstable if they disperse on approaching the fixed point [36]. In comparison to Jacobi stability analysis, Lyapunov approach is therefore more convenient to study the stability analysis as the linearization of nonlinear system takes place around a fixed point so-called equilibrium point.

Both methods of stability analysis are extensively discussed and implemented to illustrate the stability of circular orbits in the vicinity of SBH spacetime by Hossein [35]. However, the Jacobi stability of dynamical systems employing KCC theory has already been analyzed in diverse situations [36,42–45]. We shall adopt the Lyapunov stability criteria to analyse the stability in our specified background geometry. A mathematical treatment of the concept of Lyapunov stability for a dynamical system has been discussed previously (see section-2 in [35]).

2 Geodesics around TWH geometry with massless conformally coupled scalar field

This section is devoted to study the particle motion around a TWH spacetime obtained for an appropriate choice of parameters $\left(\chi = \frac{\pi}{3}, \Delta \neq \frac{\pi}{2}\right)$. Since a three parameter family of solution space is invariant under the transformation $(\eta, \chi, \Delta) \rightarrow (\eta, -\chi, -\Delta)$. Under transformation $\chi \rightarrow -\chi$, the JNWW solutions carry obvious symmetries with $\phi_m = -\phi_m$. However, for the transformation $(\eta, \chi, \Delta) \rightarrow (-\eta, \chi + \pi, \Delta)$, an additional symmetry is obtained under the coordinate transformation $r \rightarrow \tilde{r} = r - 2\eta$ (with $\phi_m = +\phi_m$). Therefore, one can consider $\eta \geq 0$ and $\chi = [0, \pi]$

without loss of generality in view of these two symmetries. Nevertheless, only those geometries are examined in which $\Delta \neq \pi$ because they do not possess an asymptotic flat region as $r \to \infty$. Furthermore, the behavior of Ricci tensor component R_{tt} as r approaches 2η shows the divergence of geometry except for the parameter values $\chi = 0, \{\chi = \frac{\pi}{3}, \Delta \neq \frac{\pi}{2}\}$, $\{\chi = \frac{2\pi}{3}, \Delta = \frac{\pi}{2}\}$ and $\chi = \pi$. The geometries are found with a naked curvature singularity at $r = 2\eta$ for other than these parameter sets [19,20]. Therefore, for our choice of parameters $\{\chi = \frac{\pi}{3}, \Delta \neq \frac{\pi}{2}\}$, the geometry can be extended beyond $r = 2\eta$ which reveals the existence of a genuine wormhole solution.

It is convenient to transform the radial coordinate r into a new isotropic radial coordinate $\bar{r}$ by the relation [19,20]

$$r = \bar{r}\left(1 + \frac{\eta}{2\bar{r}}\right)^2, \tag{10}$$

where $\bar{r}$ ranges from $\frac{\eta}{2}$ to ∞. Thus the metric conformal to the JNWW metric of TWH, supported by a massless conformally coupled scalar field, is then represented as [19]

$$ds^2 = \left[\gamma_+\left(\frac{1-\frac{\eta}{2\bar{r}}}{1+\frac{\eta}{2\bar{r}}}\right) + \gamma_-\right]^2 \left[-dt^2 + \left(1+\frac{\eta}{2\bar{r}}\right)^4 \times \left[d\bar{r}^2 + \bar{r}^2\left(d\theta^2 + \sin^2\theta d\phi^2\right)\right]\right]. \tag{11}$$

Now we investigate the geodesic motion of test particles in the equatorial plane of the TWH spacetime using Lagrangian approach. The Lagrangian for the motion (setting $\theta = \frac{\pi}{2}$) is given by

$$2\mathcal{L} = \left[\gamma_+\left(\frac{1-\frac{\eta}{2\bar{r}}}{1+\frac{\eta}{2\bar{r}}}\right) + \gamma_-\right]^2 \left[-\dot{t}^2 + \left(1+\frac{\eta}{2\bar{r}}\right)^4 \times \left(\dot{\bar{r}}^2 + \bar{r}^2\dot{\phi}^2\right)\right], \tag{12}$$

where, a overdot represents differentiation w.r.t. the affine parameter τ. The spacetime metric admits time translational symmetry (i.e. independent of t) and rotational symmetry (i.e. independent of ϕ) due to which corresponding generalized momenta are constants of motion. Using the Euler-Lagrange equations of motion, we deduce the first integral of geodesics equation for t and ϕ by introducing two conserved quantities energy (E) and angular momentum (L), measured for unit mass of a test particle as

$$\dot{t} = \frac{E}{\left[\gamma_+\left(\frac{1-\frac{\eta}{2\bar{r}}}{1+\frac{\eta}{2\bar{r}}}\right) + \gamma_-\right]^2}, \tag{13}$$

$$\dot{\phi} = \frac{L}{\left[\gamma_+\left(\frac{1-\frac{\eta}{2\bar{r}}}{1+\frac{\eta}{2\bar{r}}}\right) + \gamma_-\right]^2 \left(1+\frac{\eta}{2\bar{r}}\right)^4 \bar{r}^2}. \tag{14}$$

For convenience, we define two quantities as

$$\left(\gamma_+\left(\frac{1-\frac{\eta}{2\bar{r}}}{1+\frac{\eta}{2\bar{r}}}\right) + \gamma_-\right) = \Theta, \tag{15}$$

$$\left(1+\frac{\eta}{2\bar{r}}\right) = \Pi. \tag{16}$$

The geodesics of test particles are constrained by the equation

$$\Theta^2\left[-\dot{t}^2 + \Pi^4\left(\dot{\bar{r}}^2 + \bar{r}^2\dot{\phi}^2\right)\right] = k. \tag{17}$$

One can obtain timelike and null geodesics for $k = -1$ and $k = 0$ respectively with metric signature $(-+++)$. On substituting Eqs. (13) and (14) into constraint Eq. (17), the radial equation for geodesics in the specified spacetime is derived as

$$\Theta^4\,\Pi^4\,\frac{\dot{\bar{r}}^2}{2} = \frac{E^2}{2} - \frac{1}{2}\left(-k\,\Theta^2 + \frac{L^2}{\bar{r}^2\,\Pi^4}\right). \tag{18}$$

The radial motion of the test particle on geodesics represented by Eq. (18) is considered to be motion of a particle (with energy $E^2/2$) in the context of Newtonian mechanics moving in the effective potential V_{eff}. Therefore one can identify the above equation as a Newtonian central force problem which reads

$$\frac{\dot{\bar{r}}^2}{2} = \tilde{E} - V_{eff}(\bar{r}). \tag{19}$$

The derivative of Eq. (19) with respect to affine parameter τ gives

$$\ddot{\bar{r}} = -V'_{eff}(\bar{r}). \tag{20}$$

Here and throughout the work, ($'$) denotes differentiation w.r.t. radial coordinate. Further, we are looking for Lyapunov stability analysis of geodesics by transforming the one-dimensional radial Eq. (20) to a first order differential equation system in $\bar{r} - p$ phase-space as follows

$$\dot{\bar{r}} = p\ ,\ \dot{p} = -V'_{eff}(\bar{r}). \tag{21}$$

Hence Eq. ((19)) reduces to the following form

$$\frac{p^2}{2} + V_{eff}(\bar{r}) = \tilde{E}. \tag{22}$$

Now we consider a vector field for the system of Eqs. (21) in order to linearize the above Eq. (22) as

$$F(\bar{r}, p) = \left(p, V'_{eff}(\bar{r})\right). \tag{23}$$

At any point $(\bar{r}, p)$, one can find the Jacobian matrix of F as

$$J = \frac{\partial F(\bar{r}, p)}{\partial q} = \begin{bmatrix} 0 & 1 \\ -V''_{eff}(\bar{r}) & 0 \end{bmatrix}, \tag{24}$$

where, q is a generalized coordinate. The characteristic equation $|J - \lambda I| = 0$ yields the eigenvalues of Jacobian J as follows

$$\lambda = \pm\sqrt{-V''_{eff}(\bar{r})}. \tag{25}$$

Assuming a equilibrium point or a fixed point $(\bar{r}_0, 0)$, the $V'_{eff}(\bar{r}_0)$ vanishes, and for which $V''_{eff}(\bar{r}_0) \neq 0$. We can characterize the fixed point $(\bar{r}_0, 0)$ as a saddle point corresponding to $V''_{eff}(\bar{r}_0) < 0$ for which λ is real and a possible center corresponding to $V''_{eff}(\bar{r}_0) > 0$ for which λ is imaginary. In other words, we can say that when the potential has a local maximum at $\bar{r}_0$ then $(\bar{r}_0, 0)$ is said to be a saddle point, and when the potential has local minimum at $\bar{r}_0$ then $(\bar{r}_0, 0)$ is said to be a possible center. In particular, the energy function (22) can be interpreted as a Lyapunov function $\tilde{E}(\bar{r}, p)$. The other required condition on the Lyapunov function is that there should be a local minimum of $\tilde{E}$ at the fixed point for which the Hessian matrix can be written as [35]

$$H_{\tilde{E}} = \frac{\partial^2 \tilde{E}(\bar{r}, p)}{\partial \bar{r} \partial p} = \begin{bmatrix} V''_{eff}(\bar{r}) & 0 \\ 0 & 1 \end{bmatrix}. \tag{26}$$

Indeed, the fixed point $(\bar{r}_0, 0)$ can be identified as a possible center as the above matrix is positive definite for $V''_{eff}(\bar{r}_0) > 0$. Therefore, the Lyapunov function has a local minimum at that point. Interestingly, the fixed point $(\bar{r}_0, 0)$ is Lyapunov stable for $V''_{eff}(\bar{r}_0) > 0$ and Lyapunov unstable for $V''_{eff}(\bar{r}_0) < 0$.

In order to classify the possible orbits of test particles around TWH spacetime, we need two coordinate transformations (see [20] for details) by introducing a radial coordinates as follows

$$\hat{x} = \frac{\bar{r}}{\eta} + \frac{1}{2}, \tag{27}$$

and then transform $\hat{x}$ by

$$\hat{r} = \frac{1}{2\hat{x}}. \tag{28}$$

The new radial coordinate $\hat{r} \in [0, 1]$ and the location of the throat of TWH is then given by [20]

$$\hat{r}_T = \frac{1}{\sqrt{|(\bar{\gamma_+} - 1)/(\bar{\gamma_+} + 1)|} + 1}. \tag{29}$$

On substituting the scaled quantities $\bar{\gamma_+} = \gamma_+/\gamma_-$ and $\tilde{L} = L/\eta\gamma_-$ with transformation Eqs. (27) and (28) into V_{eff} (i.e. Eq. (19)), the effective potential in terms of the new radial coordinate $\hat{r}$ takes the following form

$$V_{eff}(\hat{r}) = 2\tilde{L}^2\hat{r}^2(1-\hat{r})^2 - \frac{k}{2}[\bar{\gamma_+}(2\hat{r} - 1) - 1]^2. \tag{30}$$

Hence the effective potential for TWH spacetime, conformally coupled to massless scalar field, has a centrifugal part and a gravitational part represented by the first and second terms of the above equation respectively.

2.1 Lyapunov stability of timelike circular orbits

In this section, we analyse the stability of timelike circular geodesics. Considering $k = -1$, Eq. (30) leads to the effective potential for the case of timelike geodesics as

$$V^T_{eff}(\hat{r}) = 2\tilde{L}^2\hat{r}^2(1-\hat{r})^2 + \frac{1}{2}[\bar{\gamma_+}(2\hat{r} - 1) - 1]^2. \tag{31}$$

Willenborg et al. [20] has already investigated and classified the types of orbits in the background of the TWH geometry, supported by a massless conformally coupled scalar field, via illustrating the effective potential. For timelike case, depending upon the various values of the angular momentum $\tilde{L}$ and TWH parameter $\bar{\gamma_+}$ (see Fig. 1 of ref. [20] for the dependency of characteristic values of $\tilde{L}$ on $\bar{\gamma_+}$), we have depicted four different types of effective potential $V^T_{eff}(\hat{r})$ in Fig. 1. The two characteristic values of angular momentum namely critical angular momentum $\tilde{L_C}$ and $\tilde{L_S}$ which obeys $V^T_{eff}(\bar{\gamma_+}, \tilde{L_S}) > V^T_{eff}(\bar{\gamma_+}, 0)$ for timelike geodesics were introduced in [20]. On this basis, four different cases arise for timelike geodesics and the orbits are classified in terms of the nature of the effective potential as follows:

Case I: when $\tilde{L} < \tilde{L}_C$ i.e. $\tilde{L} = 2.2$, only transit and escape orbits are found as the potential decreases monotonically.

Case II: when $\tilde{L} = \tilde{L}_C$ i.e. $\tilde{L} = 2.5$, the unstable circular, transit and escape orbits may exist because the potential consists a double zero in allowed range of $\hat{r}$.

Case III: when $\tilde{L}_C < \tilde{L} \leq \tilde{L}_S$ i.e. $\tilde{L} = 2.8$, the bound orbits may also be found due to minimum of effective potential, and unstable circular orbits exist due to the maximum of effective potential.

Case IV: when $\tilde{L} > \tilde{L}_S$ i.e. $\tilde{L} = 3.3$, the bound and unstable circular orbits are found along with other orbits because the maximum of potential becomes larger than $V^T_{eff}(\hat{r} = 0)$.

To determine the fixed points of the timelike effective potential, let us take $\left(V^T_{eff}(\hat{r})\right)' = 0$ and obtain these points shown in Table 1. Since in case of our spacetime metric, the radial coordinate $\hat{r} \in [0, 1]$, therefore only the fixed point $(\hat{r_0}, 0)$ within this range need to be considered.

The eigenvalues of the Jacobian matrix for the timelike case are given by

$$\lambda_T = \pm\sqrt{-\left(V^T_{eff}(\hat{r_0})\right)''}. \tag{32}$$

Further, by performing the Lyapunov stability criteria, the classification of fixed points $(\hat{r_0}, 0)$ for each case are presented in Table 2. For the cases $\tilde{L} < \tilde{L}_C$ and $\tilde{L} = \tilde{L}_C$, no fixed point belongs in the range $[0, 1]$ which reveals that the circular orbits (stable or unstable) do not exist in this range. However, for $\tilde{L}_C < \tilde{L} \leq \tilde{L}_S$, the fixed point $(0.163923, 0)$ is Lyapunov stable as the corresponding eigenvalue is imaginary while fixed point $(0.330947, 0)$ is Lyapunov unstable as the corresponding eigenvalue is real. On the other hand, for $\tilde{L} > \tilde{L}_S$, the fixed point $(0.0982812, 0)$ is Lyapunov stable as the corresponding eigenvalue is imaginary and $(0.397913, 0)$ is Lyapunov unstable as corresponding eigenvalue is real.

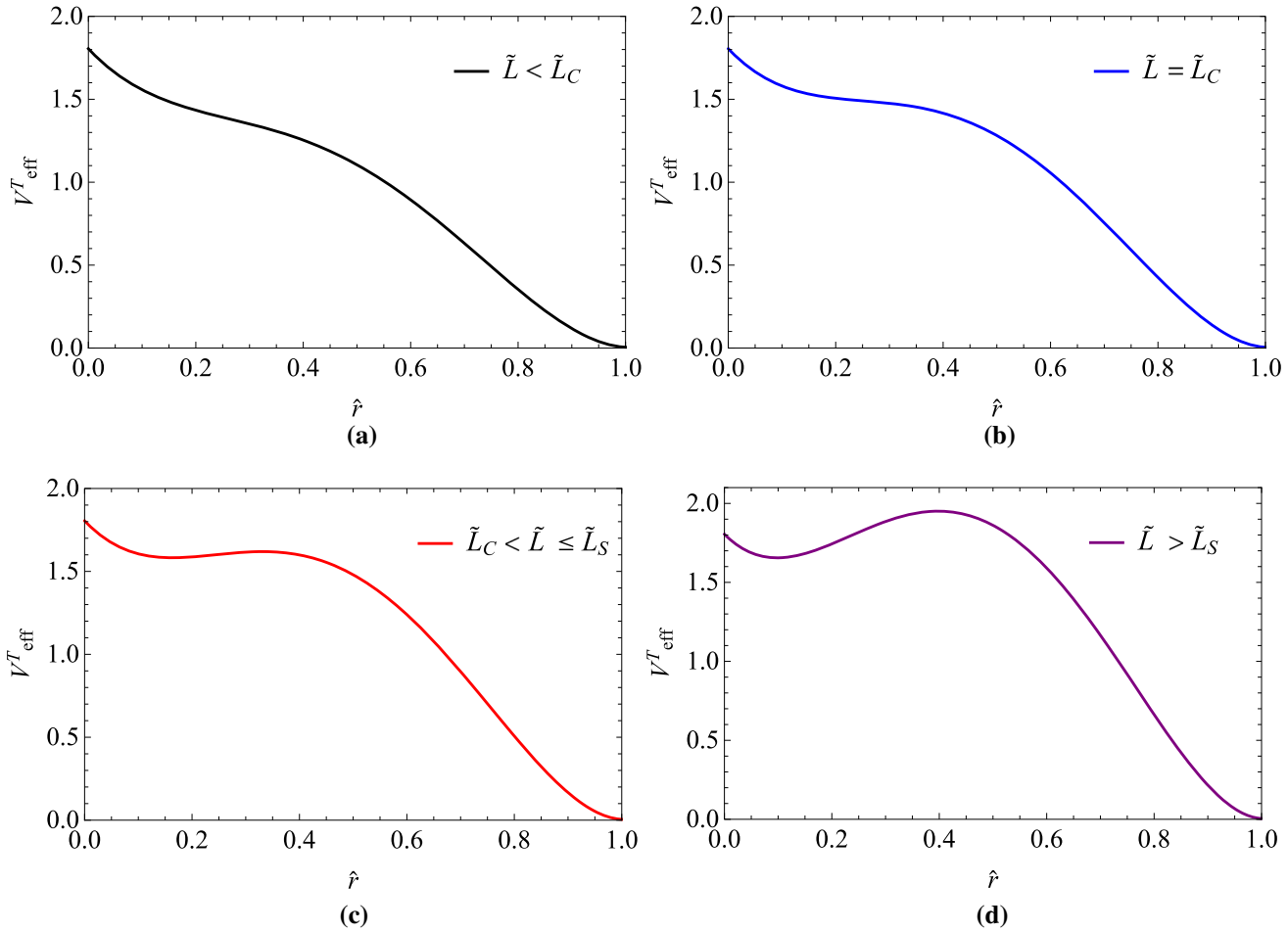

Fig. 1 Variation of effective potential $V^T_{eff}(\hat{r})$ for timelike geodesics as a function of radial coordinate $\hat{r}$ for different values of angular momentum **a** $\tilde{L} = 2.2$, **b** $\tilde{L} = 2.5$, **c** $\tilde{L} = 2.8$ and **d** $\tilde{L} = 3.3$. Here we fix the TWH parameter $\bar{\gamma_+}$ to 0.9

Table 1 Fixed points $(\hat{r_0}, 0)$ of $V^T_{eff}(\hat{r})$ for timelike geodesics for different cases with $\bar{\gamma_+} = 0.9$

$\tilde{L} < \tilde{L}_C$	$\tilde{L} = \tilde{L}_C$	$\tilde{L}_C < \tilde{L} \leq \tilde{L}_S$	$\tilde{L} > \tilde{L}_S$
0.246096 + 0.164556 i	0.246865 + 0.083853 i	0.163923	0.0982812
0.246096 − 0.164556 i	0.246865 − 0.083853 i	0.330947	0.397913
1.00781	1.00627	1.00513	1.00381

Table 2 Lyapunov stability of fixed points $(\hat{r_0}, 0)$ for different cases in timelike geodesics

Case	Fixed point $(\hat{r_0}, 0)$	$\left(V^T_{eff}(\hat{r_0})\right)''$	λ_T	Lyapunov stability
$\tilde{L}_C < \tilde{L} \leq \tilde{L}_S$	0.163923	8.81225	Imaginary	Lyapunov stable
	0.330947	−7.06259	Real	Lyapunov unstable
$\tilde{L} > \tilde{L}_S$	0.0982812	23.6378	Imaginary	Lyapunov stable
	0.397913	−15.8162	Real	Lyapunov unstable

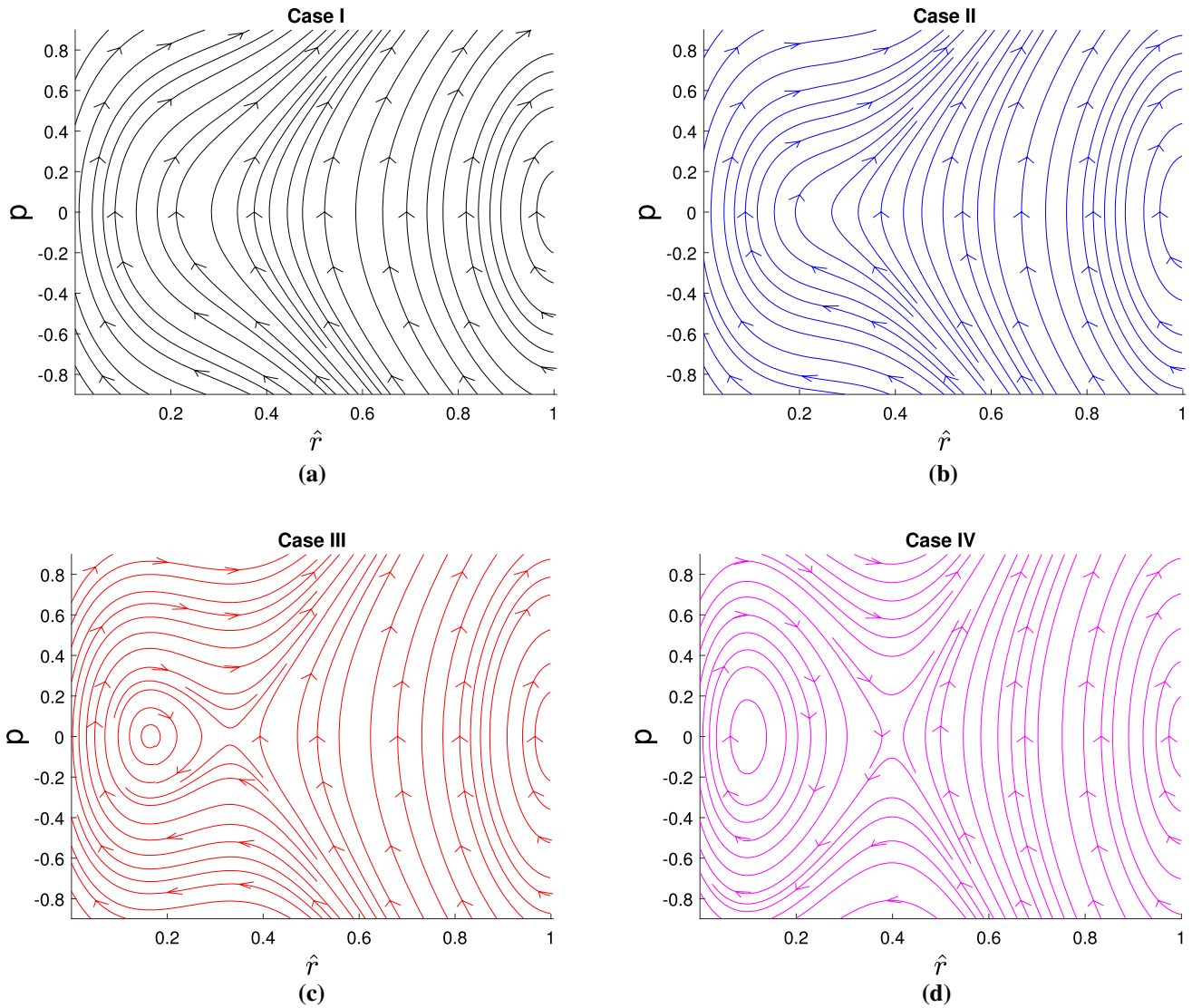

Fig. 2 The phase portrait in $\hat{r} - p$ plane for four different cases of angular momentum $\tilde{L}$ for timelike geodesics with parameter $\gamma_+^- = 0.9$.

A circular orbit exists corresponding to each fixed point of the effective potential for timelike as well as null geodesics. Furthermore, one can also differentiate the circular orbits at fixed points as saddle point (which is Lyapunov unstable) and stable center (which is Lyapunov stable) by visualizing the phase portrait. The phase portrait in $\hat{r} - p$ plane for stable and unstable timelike circular orbits are shown in Fig. 2. It is observed that

Case I ($\tilde{L} < \tilde{L}_C$): as shown in Fig. 2a, the stable or unstable circular orbits are not found because no fixed point exists within range [0, 1].

Case II ($\tilde{L} = \tilde{L}_C$): it is clearly shown in Fig. 2b, that stable or unstable circular orbits are not found as no fixed point lies within range [0, 1].

Case III ($\tilde{L}_C < \tilde{L} \leq \tilde{L}_S$): from the corresponding phase portrait presented in Fig. 2c, we observe that the circular orbit at fixed point (0.163923, 0) is a stable center, while another circular orbit at fixed point (0.330947, 0) is an unstable saddle point.

Case IV ($\tilde{L} > \tilde{L}_S$): from Fig. 2d, one can notice that the circular orbit at fixed point (0.163923, 0) is a stable center while another circular orbit at fixed point (0.330947, 0) is an unstable saddle point.

2.2 Lyapunov stability of null circular orbits

From Eq. (30), if $k = 0$ is taken into account, the effective potential for null circular geodesics that contains only the centrifugal part is expressed as

$$V_{eff}^N(\hat{r}) = 2\tilde{L}^2\hat{r}^2(1-\hat{r})^2. \tag{33}$$

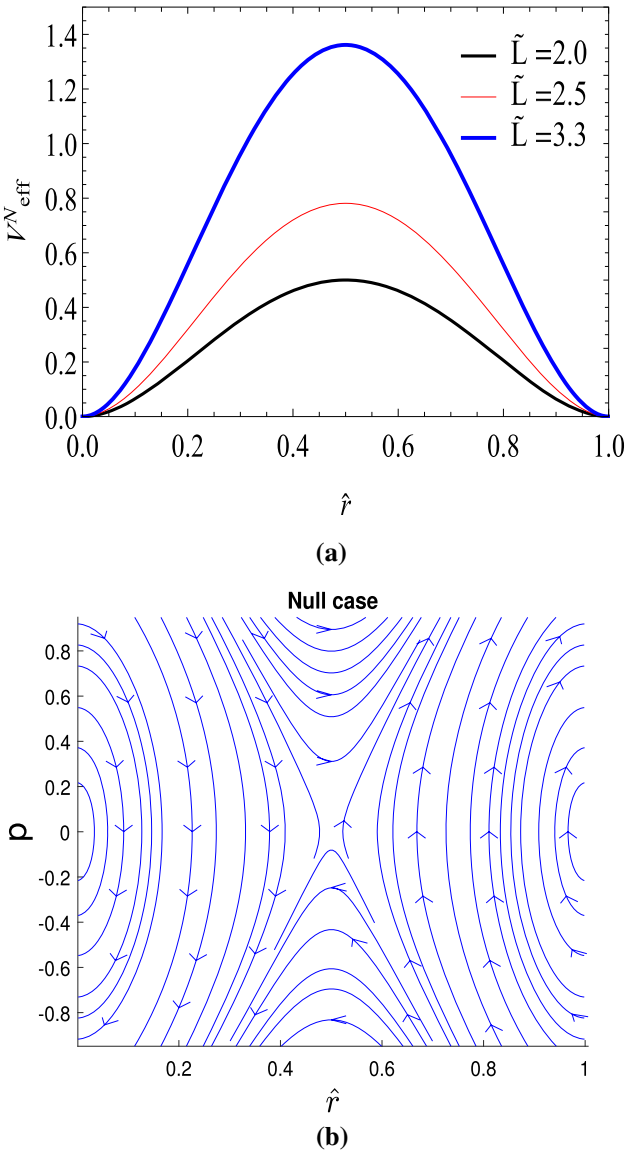

Fig. 3 **a** Variation of the effective potential V^N_{eff} for null geodesics as a function of radial coordinate $\hat{r}$ for different values of $\tilde{L}$. **b** The phase portrait in $\hat{r} - p$ plane with angular momentum $\tilde{L} = 3.3$ for null geodesics

It is straight forward to note that the effective potential depends only on angular momentum $\tilde{L}$ and is independent of the parameter γ_+^- i.e. the effect of TWH parameter is insignificant. The behavior of the effective potential V^N_{eff} versus $\hat{r}$ presented in Fig. 3a, shows that the height of the potential depends on the size of the angular momentum $\tilde{L}$. In the asymptotic regions i.e. $\hat{r} = 0, 1$, the potential V^N_{eff} vanishes and possesses a maximum at $\hat{r} = 0.5$. Hence, the types of orbits are likely to be transit and escape orbits along with unstable circular orbits for the null case.

By using the condition $\left(V^N_{eff}\right)' = 0$, we have determined the fixed point $(\hat{r_*}, 0)$ for null circular geodesics as $(0, 0)$, $(0.5, 0)$ and $(1, 0)$. The Jacobian matrix for null geodesics is thus obtained giving eigenvalues corresponding to each fixed point as

$$\lambda_N = \pm\sqrt{-\left(V^N_{eff}(\hat{r_*})\right)''}. \tag{34}$$

The Lyapunov stability of each fixed point for the fixed value of angular momentum $\tilde{L} = 3.3$ is visualised in Table 3. The fixed point $(0.5, 0)$ is Lyapunov unstable as eigenvalues at this point is real while the other two points are Lyapunov stable as eigenvalues at these point are imaginary. Besides, we have visualized the phase-portrait in Fig. 3b in order to decide whether the circular orbits at fixed points are stable center or a saddle point. Nevertheless, the radial coordinate $\hat{r}$ can vary from 0 to 1, and fixed asymptotic points $(0, 0)$ and $(1, 0)$ are not considered for corresponding circular orbits to be stable center. Clearly, it is observed from the phase portrait that the circular orbit at only the fixed point $(0.5, 0)$ is an unstable saddle point. Consequently, it can noticed that no stable circular orbits exist in the range $0 < \hat{r} < 1$ and an unstable circular orbit of photons (lightlike particle) exists only at $\hat{r} = 0.5$.

3 Conclusion

We have explored the Lyapunov stability analysis of circular orbits in gravitational field of a TWH geometry, conformally coupled to a massless scalar field, which is introduced by a"new improved stress-energy tensor". Instead of the NEC violation, such WH geometry stay with GR describes gravity without any exotic type of matter distribution. Subsequently, we investigated the stability of both particle (timelike) and photon (null) orbits in detail. Based on our study, we have differentiated the fixed points according to their Lyapunov stability of effective potential for both timelike and null geodesics. For timelike geodesics, on classifying the the four different types of effective potentials (in view of conditions to angular momentum $\tilde{L}$), there are no fixed points obtained in the range of radial coordinate $0 \leq \hat{r} \leq 1$ for the cases $\tilde{L} < \tilde{L}_C$ and $\tilde{L} = \tilde{L}_C$. However, for $\tilde{L}_C < \tilde{L} \leq \tilde{L}_S$, we found $(0.163923, 0)$ as a Lyapunov stable point and $(0.0.330947, 0)$ as a Lyapunov unstable point. Also in the case of $\tilde{L} > \tilde{L}_S$, the fixed points $(0.0982812, 0)$ and $(0.397913, 0)$ are found to be Lyapunov stable and unstable respectively. Indeed, each fixed point of the effective potential is referred as a circular orbit of a particle about the origin. Further, by visualizing the corresponding $(\hat{r} - p)$ phase-portrait, we observed that the timelike circular orbit at every fixed point is either a stable center or an unstable saddle point (visualized in the corresponding phase-space diagrams). Turning to lightlike particles (photons), by deducing the effective potential, the fixed points $(0, 0)$ and $(1, 0)$ are

Table 3 Lyapunov stability of fixed points $(\hat{r_*}, 0)$ for angular momentum $\tilde{L} = 3.3$ in null geodesics

Fixed point $(\hat{r_*}, 0)$	$\left(V_{eff}^{N}(\hat{r_*})\right)''$	λ_N	Lyapunov stability
(0, 0)	43.56	Imaginary	Lyapunov stable
(0.5, 0)	− 21.78	Real	Lyapunov unstable
(1, 0)	43.56	Imaginary	Lyapunov stable

identified as Lyapunov stable while only one point (0.5, 0) is found to be Lyapunov unstable. The phase-portrait regarding null geodesics also revealed that the null circular orbit at the Lyapunov unstable fixed point (i.e. 0.5, 0) is obtained as a saddle point. As a consequence, we note that stable circular orbits do not exist for the case of null geodesics.

Acknowledgements S.G. gratefully acknowledges University Grants Commission (UGC), New Delhi, India for providing the financial support as a Senior Research Fellow through UGC-Ref.No. 1479/CSIR-UGC NET-JUNE2017. The authors also acknowledge the facilities available at ICARD, Gurukula Kangri (Deemed to be University) Haridwar those were used during the course of this work.

Data Availability Statement This manuscript has no associated data or the data will not be deposited. [Authors' comment: The paper is purely theoretical research. There is no accompanying data in the manuscript.]

Open Access This article is licensed under a Creative Commons Attribution 4.0 International License, which permits use, sharing, adaptation, distribution and reproduction in any medium or format, as long as you give appropriate credit to the original author(s) and the source, provide a link to the Creative Commons licence, and indicate if changes were made. The images or other third party material in this article are included in the article's Creative Commons licence, unless indicated otherwise in a credit line to the material. If material is not included in the article's Creative Commons licence and your intended use is not permitted by statutory regulation or exceeds the permitted use, you will need to obtain permission directly from the copyright holder. To view a copy of this licence, visit http://creativecommons.org/licenses/by/4.0/.
Funded by SCOAP[3].

References

1. A. Einstein, N. Rosen, The particle problem in the general theory of relativity. Phys. Rev. **48**(1), 73 (1935)
2. M. Visser, *Lorentzian Wormholes* (From Einstein to Hawking, Woodbury, 1995)
3. M.S. Morris, K.S. Thorne, Wormholes in spacetime and their use for interstellar travel: a tool for teaching general relativity. Am. J. Phys. **56**(5), 395–412 (1988)
4. J.G. Cramer, R.L. Forward, M.S. Morris, M. Visser, G. Benford, G.A. Landis, Natural wormholes as gravitational lenses. Phys. Rev. D **51**(6), 3117 (1995)
5. V. Perlick, Exact gravitational lens equation in spherically symmetric and static spacetimes. Phys. Rev. D **69**(6), 064017 (2004)
6. M. Safonova, D.F. Torres, G.E. Romero, Microlensing by natural wormholes: theory and simulations. Phys. Rev. D **65**(2), 023001 (2001)
7. P.K.F. Kuhfittig, Gravitational lensing of wormholes in the galactic halo region. Eur. Phys. J. C **74**(3), 1–6 (2014)
8. T. Ohgami, N. Sakai, Wormhole shadows. Phys. Rev. D **91**(12), 124020 (2015)
9. P.G. Nedkova, V.K. Tinchev, S.S. Yazadjiev, Shadow of a rotating traversable wormhole. Phys. Rev. D **88**(12), 124019 (2013)
10. R. Shaikh, Shadows of rotating wormholes. Phys. Rev. D **98**(2), 024044 (2018)
11. C. Bambi, Broad k α iron line from accretion disks around traversable wormholes. Phys. Rev. D **87**(8), 084039 (2013)
12. T. Harko, Z. Kovács, F.S.N. Lobo, Electromagnetic signatures of thin accretion disks in wormhole geometries. Phys. Rev. D **78**(8), 084005 (2008)
13. T. Harko, Z. Kovacs, F.S.N. Lobo, Thin accretion disks in stationary axisymmetric wormhole spacetimes. Phys. Rev. D **79**(6), 064001 (2009)
14. T. Damour, S.N. Solodukhin, Wormholes as black hole foils. Phys. Rev. D **76**(2), 024016 (2007)
15. V. Cardoso, E. Franzin, P. Pani, Erratum: Is the gravitational-wave ringdown a probe of the event horizon? (Phys. Rev. Lett. 116, 171101 (2016)). Phys. Rev. Lett. **117**(8):089902 (2016)
16. P. Bueno, P.A. Cano, F. Goelen, T. Hertog, B. Vercnocke, Echoes of Kerr-like wormholes. Phys. Rev. D **97**(2), 024040 (2018)
17. S.W. Hawking, G.F.R. Ellis, *The Large Scale Structure of Space-time*, vol. 1 (Cambridge University Press, Cambridge, 1973)
18. F.S.N. Lobo, *Wormholes, Warp Drives and Energy Conditions*, vol. 189 (Springer, Berlin, 2017)
19. C. Barcelo, M. Visser, Traversable wormholes from massless conformally coupled scalar fields. Phys. Lett. B **466**(2–4), 127–134 (1999)
20. F. Willenborg, S. Grunau, B. Kleihaus, J. Kunz, Geodesic motion around traversable wormholes supported by a massless conformally coupled scalar field. Phys. Rev. D **97**(12), 124002 (2018)
21. C.G. Böhmer, T. Harko, F.S.N. Lobo, Wormhole geometries with conformal motions. Class. Quantum Gravity **25**(7), 075016 (2008)
22. E.E. Flanagan, R.M. Wald, Does back reaction enforce the averaged null energy condition in semiclassical gravity? Phys. Rev. D **54**(10), 6233 (1996)
23. H.G. Ellis, The evolving, flowless drainhole: a nongravitating-particle model in general relativity theory. Gen. Relativ. Gravit. **10**(2), 105–123 (1979)
24. B. Kleihaus, J. Kunz, Rotating Ellis wormholes in four dimensions. Phys. Rev. D **90**(12), 121503 (2014)
25. X.Y. Chew, B. Kleihaus, J. Kunz, Geometry of spinning ellis wormholes. Phys. Rev. D **94**(10), 104031 (2016)
26. H. Fukutaka, K. Ghoroku, K. Tanaka, Wormholes solutions in higher derivative gravity. Phys. Lett. B **222**(2), 191–194 (1989)
27. F.S.N. Lobo, M.A. Oliveira, Wormhole geometries in f (r) modified theories of gravity. Phys. Rev. D **80**(10), 104012 (2009)
28. P. Kanti, B. Kleihaus, J. Kunz, Wormholes in dilatonic Einstein–Gauss–Bonnet theory. Phys. Rev. Lett. **107**(27), 271101 (2011)
29. T. Harko, F.S.N. Lobo, M.K. Mak, S.V. Sushkov, Modified-gravity wormholes without exotic matter. Phys. Rev. D **87**(6), 067504 (2013)
30. C.G. Callan Jr., S. Coleman, R. Jackiw, A new improved energy-momentum tensor. Ann. Phys. **59**(1), 42–73 (1970)
31. A.I. Janis, E.T. Newman, J. Winicour, Reality of the schwarzschild singularity. Phys. Rev. Lett. **20**(16), 878 (1968)

32. M. Wyman, Static spherically symmetric scalar fields in general relativity. Phys. Rev. D **24**(4), 839 (1981)
33. K.S. Virbhadra, Janis-Newman-Winicour and Wyman solutions are the same. Int. J. Mod. Phys. A **12**(27), 4831–4835 (1997)
34. A.G. Agnese, M. La Camera, Gravitation without black holes. Phys. Rev. D **31**(6), 1280 (1985)
35. H. Abolghasem, Stability of circular orbits in schwarzschild spacetime. Int. J. Differ. Equ. Appl. **12**(3), (2013)
36. C.G. Boehmer, T. Harko, S.V. Sabau, Jacobi stability analysis of dynamical systems-applications in gravitation and cosmology. Adv. Theor. Math. Phys. **16**(4), 1145–1196 (2012)
37. H. Abolghasem, Liapunov stability versus jacobi stability. J. Dyn. Syst. Geom. Theor. **10**(1), 13–32 (2012)
38. H. Abolghasem, Jacobi stability of circular orbits in a central force. J. Dyn. Syst. Geom. Theor. **10**(2), 197–214 (2012)
39. DD Kosambi, Parallelism and path-spaces, in *DD Kosambi* (Springer, 2016), p. 59–70.
40. É. Cartan, Observations sur le mémoire précédent, in *DD Kosambi*, (Springer 2016), p. 71–74.
41. S.-S. Chern, Sur la géométrie d'un système d'équations différentielles du second ordre [on the geometery of a system of second order differential equations]. Bull. Sci. Math., II. Ser., 63:206–212, 1939. MR:0000889. Zbl:0023.07701
42. V. Balan, I.R. Nicola, Berwald-moor metrics and structural stability of conformally-deformed geodesic sode. Appl. Sci. **11** (2009)
43. C.G. Boehmer, T. Harko, Nonlinear stability analysis of the Emden-Fowler equation. J. Nonlinear Math. Phys. **17**(4), 503–516 (2010)
44. T. Harko, V.S. Sabau, Jacobi stability of the vacuum in the static spherically symmetric brane world models. Phys. Rev. D **77**(10), 104009 (2008)
45. S.V. Sabau, Some remarks on jacobi stability. Nonlinear Anal. Theory Methods Appl. **63**(5–7), e143–e153 (2005)